

Modeling of a G_c -sensing element for the interfacial toughness of metal thin films on substrates

Insu Jeon^{a,*}, Masaki Omiya^b, Kikuo Kishimoto^b, Tadashi Asahina^a, Seyoung Im^c

^a *Materials Research Institute for Sustainable Development, National Institute of Advanced Industrial Science and Technology (AIST), Shimoshidami, Moriyama-ku, Nagoya 463-8560, Japan*

^b *Department of Mechanical and Control Engineering, Tokyo Institute of Technology, O-okayama, Meguro-ku, Tokyo 152-8552, Japan*

^c *Department of Mechanical Engineering, Korea Advanced Institute of Science and Technology (KAIST), Science Town, Daejeon 305-701, South Korea*

Received 11 July 2004; received in revised form 14 January 2005; accepted 23 April 2005

Available online 25 May 2005

Abstract

A new type of the sensitive specimen named ' G_c -sensing element' that can be fabricated, using the plain and general micro-fabrication process, is proposed and modeled to measure the interfacial toughness G_c of metal thin films on substrates. For the whole modeling process of the G_c -sensing element, the finite element method and the concepts of the linear elastic fracture mechanics are applied. Moreover, the verification for energy-release rates calculated from the linear elastic fracture analysis is carried out, using the elastic–plastic fracture analysis. The results of this research show that the G_c -sensing element provides a simple and convenient method for measuring the precise interfacial toughness of metal thin films on substrates.

© 2005 Elsevier B.V. All rights reserved.

Keywords: G_c -sensing element; Indentation; Metal thin films; Interfacial toughness

1. Introduction

The adhesion strength of thin films on substrates has an important effect on the reliability and lifetime of micro-scale systems, such as the high-capacity memory chip, the chip-scale package and the micro-electro-mechanical system, and it can be defined as the interfacial toughness G_c , which is a measure of the practical work of adhesion [1]. Therefore, various approaches to measure G_c for thin films have been actively performed and published up to the present [2].

Among these approaches, the research using the nanoindentation is the main stream for measuring G_c of thin films under μm -scale thickness. The indentation [3–7] or the scratch [8,9], using the nanoindentation is applied on the surface of the films, and then G_c can be obtained with its mathematical expressions and measured geometric variables, i.e., the

indentation volume, the crack length and the scratch trace geometry in the films.

In a different way, the interfacial toughness of thin films has been measured using fabricated specimens [10–13]. The superlayer test [10,11] has the originality of such measurement methods. The carbon-release layer is deposited between the Cu film and the substrate to reduce the adhesion strength, and the residual stress of the Cr superlayer deposited on the film is used as an external loading to generate the crack between the film and the substrate. The interfacial toughness, as well as the phase angle, are calculated with the residual stress, and equations are formulated on the basis of the linear elastic fracture mechanics.

Each method has some merits for measuring G_c , for example, the plain fabrication process of the test specimen, the simple calculation of the energy-release rate for the nanoindentation method, and the strong possibility to obtain the accurate G_c of thin films for the superlayer test method. On the other hand, they have serious demerits. For example,

* Corresponding author. Tel.: +81 52 736 7449; fax: + 81 52 736 7400.
E-mail address: insu-jeon@aist.go.jp (I. Jeon).

the nanoindentation method has a high probability of overestimating or underestimating G_c because of the inverse quadratic or the inverse biquadratic dependence of the measured crack length, which may include some errors during the measuring process, in the expressions of the energy-release rate [3–7]. The superlayer test method gives the difficulty of obtaining the exact value of G_c because of the hardness for controlling the external loading that creates the interfacial crack.

In this research, a new type of a sensitive specimen named ‘ G_c -sensing element’ is proposed for measuring the interfacial toughness of metal thin films on substrates to compensate for those demerits of both the methods. The plain and general micro-fabrication processes are sufficient to fabricate the G_c -sensing element. The nanoindentation or the microindentation can be utilized to apply an external loading and to probe the ‘pop-in’ point in the load–displacement curve, from which the loading for the initiation of the crack propagation is obtained. For the whole modeling process of the G_c -sensing element, the finite element method and the theory of the linear elastic fracture mechanics are applied. Also, the verification for calculated energy-release rates, obtained from the linear elastic fracture analysis, is performed with the elastic–plastic fracture analysis.

2. New type of specimen, G_c -sensing element

The geometric flexibility of thin silicon structures under 300 μm thickness, shown in Fig. 1 [14,15], is the fundamental characteristic for realizing the G_c -sensing element. Fig. 2a shows the proposed shape of the G_c -sensing element and the essential micro-fabrication processes, i.e., the oxidation of the Si substrate, the deposition of the release layer and the metal thin film, the spin-coating of the photo resist (PR) and the lithography, as well as the etching for the PR layer, the film, and the substrate. Particularly, the partial etching of the metal thin film is recommended to form a small metal contact pad of the 60 μm diameter on the center of the substrate surface, which guides the symmetric loading transfer from the indentation to the G_c -sensing element (see Fig. 2a). Also, we suggest that the etching process of the PR layer and the metal thin film on the substrate have to be finished before the backside etching of the substrate to prevent the warping or bending deformation of the G_c -sensing element after the fabrication process [16].

The crack in the G_c -sensing element can be fabricated, using the deposited release layer between the SiO_2 layer and the metal thin film, and a slight pre-loading applied on the metal contact pad by the indenter. For the release layer, various kinds of the material that reduce the interfacial adhesion strength should be used. For example, the carbon layer less than 20 nm of thickness that has been used in the fabrication of the superlayer test specimen [11], or the SAM (self-assembled monolayer) less than 2 nm of thickness [17,18] can be candidates for the layer. After the pre-loading is ap-

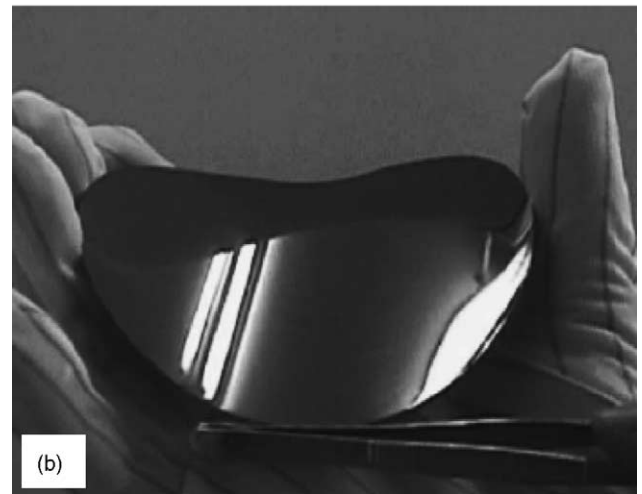
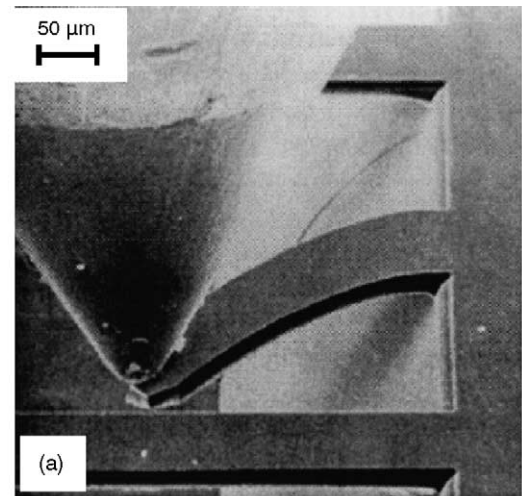


Fig. 1. The geometric flexibility of a thin Si: (a) substrate, and (b) wafer [13,14].

plied on the contact pad, the interfacial crack should be easily fabricated because of the stress concentration around the interfacial edge, as shown in Fig. 2a [16], and the low interfacial adhesion strength between the release layer and the metal thin film.

To probe the loading at the initiation of the crack propagation, i.e., the ‘pop-in’ point in the load–displacement curve, the actual indentation is processed and then the measured loading is used for calculating the interfacial toughness. During the indentation process, the external loading transferred by an indenter, bends the substrate that has the geometric flexibility, but the PR layer on the metal thin film resists the bending deformation of the film with its stiffness. Therefore, the crack between the film and the SiO_2 layer begins to propagate. Even though the external loading is applied on the metal contact pad like a point loading during the process, the plastic deformation of the pad and the bending deformation of the substrate relieve the stress concentration at the contact point, and the loading produces the uniform stress field around two cracks in the G_c -sensing element because of

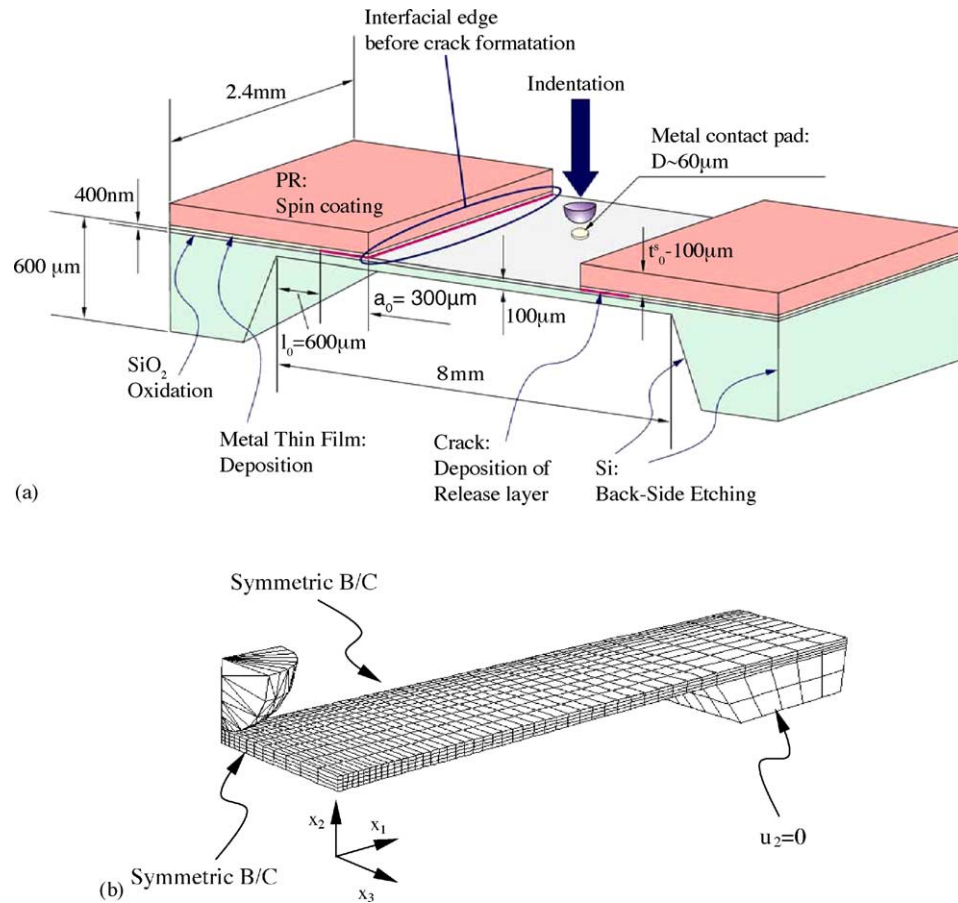


Fig. 2. (a) The proposed shape of the G_c -sensing element, and (b) the mesh configuration and boundary condition for the bridge-shaped substrate.

St. Venant's principle. Therefore, the external loading should cause the uniform propagation of the cracks.

3. Modeling of the G_c -sensing element

For modeling the G_c -sensing element, three conditions for the bridge-shaped substrate, shown in Fig. 2a, and two limitations of the indentation equipment have to be considered, which are written as follows:

- C1. Feasibility of handling.
- C2. Deflection and angle of deflection of the beam in the substrate.
- C3. Crack propagation under the plane strain deformation.

- L1. Maximum loading (f_{mx}).
- L2. Maximum displacement (d_{mx}).

The condition for the feasibility of handling means that the position and location of the G_c -sensing element have to be controlled using tweezers after being isolated from the wafer. This condition gives the degree of freedom for scrutinizing the initial and the propagated crack shape, using a microscope or a scanning electron microscope (SEM). The

condition for the deflection and the angle of deflection of the beam is needed to guarantee the crack propagation before a fracture of the beam in the substrate. The long length of the beam results in the deflection with a low probability of the beam fracture and of the crack propagation from the small angle of deflection. On the other hand, the short length of the beam results in the deflection with a high probability of the beam fracture and of the crack propagation from the large angle of deflection. Therefore, the deformation analysis for the bridge-shaped substrate, using the finite element method, is necessary for determining the reasonable size and shape of the substrate. For cracks embedded under metal thin films, the condition for the crack propagation under the plane strain deformation, $a \leq W/8$ is considered[19]. Here, W and a are the beam width and the crack length, respectively. For two limitations of the indentation equipment, $f_{\text{mx}} = 4.903 \text{ N}$ and $d_{\text{mx}} = 100 \mu\text{m}$ are selected, which are the limitations of the microindenter, MCTM-500 of SHIMADU Corp.

First of all, modeling for the bridge-shaped substrate begins under all these conditions and limitations, using the 3D finite element analysis for the indentation process. To estimate whether the substrate is fractured or not, the experimentally measured fracture strength of an Si substrate is introduced and compared with the maximum tensile stress

Table 1
Material properties for the numerical analysis

	E (GPa)	ν	Yield stress (MPa)
Si [20]	169	0.3	
SiO ₂	70	0.17	
Cu (thin film) [2]	120	0.34	400.07
SU8 (PR)	4.4	0.22	
Diamond (indenter)	900	0.2	

calculated from the numerical analysis. Because the fracture strength of an Si substrate depends not only on the crystal orientation, but also the etching process with various etchants, the minimum value of the fracture strength, 660 MPa, among published ones is used as a critical value [20]. Note that a fracture of the SiO₂ layer (see Fig. 2a) before a fracture of the Si substrate is not considered in this research because the fracture strength of an SiO₂ film is higher than that of an Si substrate introduced in this paper.

The thickness of the Si substrate 600 μm , shown in Fig. 2a, is that of a wafer before the etching process, and the beam length in the substrate is selected as 8 mm after taking into account the conditions ‘C1’ and ‘C2’. Moreover, the 400 nm thickness of the SiO₂ layer is modeled on the substrate for the fracture analysis in this research. Therefore, the variables that have to be determined by the numerical analysis are the width W and the thickness t of the beam. The mesh configuration and boundary condition for the numerical analysis are shown in Fig. 2b. For the simplicity of the computation, we disregard the small metal contact pad on the substrate, and consider only a quarter part of the substrate and the hemispherical indenter. The package code ABAQUS is employed for the finite element solution. The isoparametric hexahedron element with 20 nodes for the substrate and the tetrahedron element with four nodes for the indenter are used. As an external loading for the numerical analysis, the maximum displacement of the microindenter $d_{\text{mx}} = 100 \mu\text{m}$ is selected.

The properties of each material for the numerical analysis are shown in Table 1. As the material for the PR layer and the metal thin film, SU8 and Cu are, respectively chosen, because SU8 is used in the field of MEMS, and Cu is recently used in the semiconductor industry as metal interconnections. The simple elastic behavior for the SiO₂ layer and the Si substrate are assumed for the numerical calculation, because the actual stress field in thin films on the Si substrate can be reasonably evaluated under this assumption [21]. Particularly, Si with the same crystal direction, as the one introduced for the fracture strength, are considered for the substrate [20]. As the material of an indenter, the diamond is selected, and because of its hardness, only elastic material properties are chosen. Also, the elastic behavior of SU8 is assumed during the indentation process because the ‘ductile’ characteristic of the SU8 layer is transformed into the ‘brittle’ one after the post-exposure bake and the hard bake process [22]. The elastic and the elastic–plastic properties of the Cu thin film will be considered in following sections.

The maximum tensile stress σ_{11} is calculated at a mid-point of the lower free surface in the beam, and is compared with the fracture strength σ_f of the Si substrate. Fig. 3a and b show the ratio σ_{11}/σ_f , and the ratio f/f_{mx} between the applied loading f and the maximum loading f_{mx} , following the change of the non-dimensionalized values t/L and W/L . The values $\sigma_{11}/\sigma_f > 1$ mean a fracture of the substrate, and the values $f/f_{\text{mx}} > 1$ mean the loading that cannot be transferred by MCTM-500. In Fig. 3c, the projected σ_{11}/σ_f and f/f_{mx} values in the $t/L - W/L$ plane are shown. The improper values for reliable modeling of the substrate are excluded with the regions of oblique lines, and a suitable value for modeling is selected and marked in Fig. 3c at $t/L = 0.0125$ and $W/L = 0.3$. After selecting the beam length W , the crack length a is determined as $a = W/8$, to ensure the crack propagation under the plane strain deformation. Therefore, the determined dimensions of the bridge-shaped substrate for the G_c -sensing element are $t = 100 \mu\text{m}$, $W = 2.4 \text{ mm}$, and $a = 300 \mu\text{m}$. For the fracture analysis to calculate the energy-release rate and the phase angle using the G_c -sensing element, the thickness of the Cu film is selected as 400 nm, and the respective reference values for the geometric variables, such as the distance between the beam edge and the crack tip, the crack length and the thickness of SU8 are chosen as, $l_0 = 600 \mu\text{m}$, $a_0 = 300 \mu\text{m}$, and $t_0^S = 100 \mu\text{m}$. All of the determined dimensions and the reference geometric variables are shown in Fig. 2a, and for the reference elastic modulus of SU8, $E_0^S = 4.4 \text{ GPa}$ is selected.

4. Linear elastic fracture analysis

The stress and displacement fields around an interfacial crack tip of two isotropic elastic materials have the well-known forms [23,24]:

$$\sigma_{ij} = \frac{1}{\sqrt{2\pi r}} (\text{Re}[\mathbf{K}r^{i\varepsilon}]p_{ij}(\theta, \varepsilon) + \text{Im}[\mathbf{K}r^{i\varepsilon}]q_{ij}(\theta, \varepsilon)) \quad (1)$$

$$u_i = \frac{1}{2\mu} \sqrt{\frac{r}{2\pi}} (\text{Re}[\mathbf{K}r^{i\varepsilon}]m_i(\theta, \varepsilon) + \text{Im}[\mathbf{K}r^{i\varepsilon}]n_i(\theta, \varepsilon)) \quad (2)$$

where $i = \sqrt{-1}$, r and θ are polar coordinates centered at the crack tip, as shown in Fig. 4, $\mathbf{K} = K_1 + iK_2$ is the complex interfacial stress intensity factor, and

$$\varepsilon = \frac{1}{2\pi} \ln \left[\frac{(\kappa_1/\mu_1) + (1/\mu_2)}{(\kappa_2/\mu_2) + (1/\mu_1)} \right] \quad (3)$$

The material constants $\kappa_\alpha = 3 - 4\nu_\alpha$, μ_α and ν_α are the shear modulus and Poisson’s ratio, respectively, where the subscript ‘ α ’ means the upper layer ($\alpha = 1$) or the lower layer ($\alpha = 2$). The detailed solutions for p_{ij} , q_{ij} , m_j and n_i are given by Rice et al. [25].

The conservation integral, J -integral [26] is introduced to define the energy-release rate:

$$J = \int_{\Gamma} (Wn_1 - t_i u_{i,1}) ds \quad (4)$$

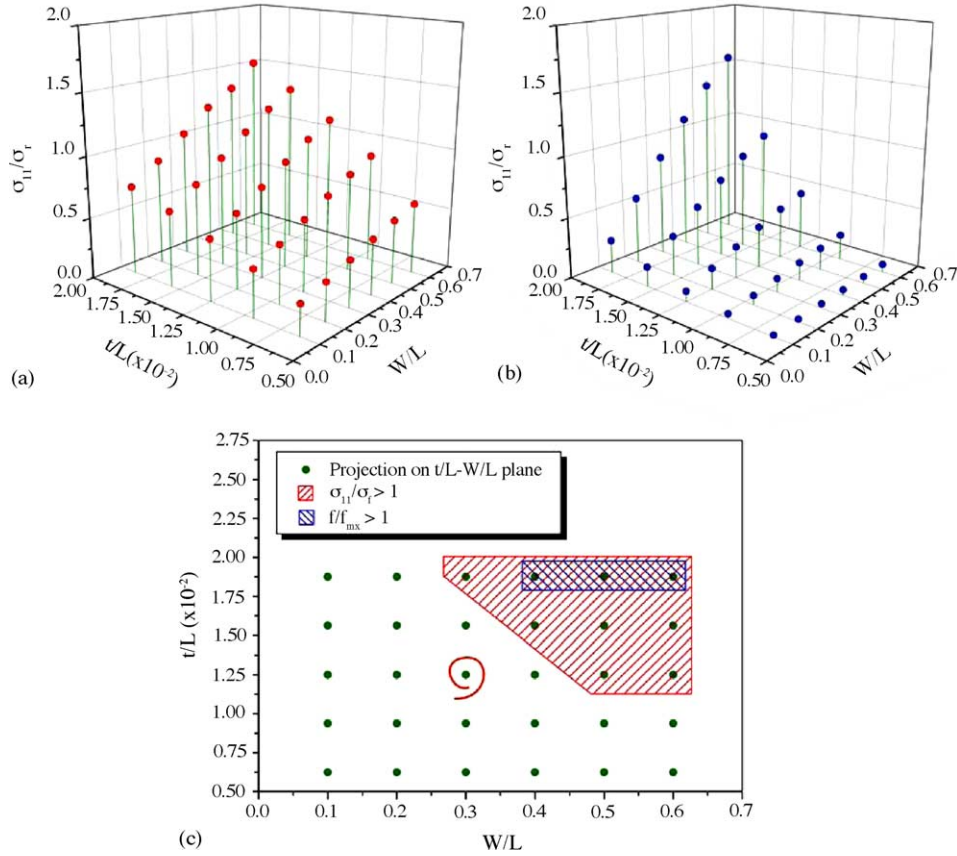


Fig. 3. The ratio (a) σ_{11}/σ_r , and (b) f/f_{max} following the change of t/L and W/L , and (c) their projected values in the $t/L - W/L$ plane ($d = 100 \mu\text{m}$).

where n_1 is the unit outward normal on the contour Γ in Fig. 4; W and t_i indicate the strain energy density and the traction component given as, $W = \sigma_{ij}\epsilon_{ij}/2$ and $t_i = \sigma_{ij}n_j$; ‘ $u_{i,1}$ ’ is the partial derivative with respect to x_1 . Here, the strain

component ϵ_{ij} is given as $\epsilon_{ij} = (u_{i,j} + u_{j,i})/2$. The calculation after substituting the stress and displacement fields in Eqs. (1) and (2) into the definition of the J -integral in Eq. (4) gives the well-known form of the energy-release rate for an elastic interfacial crack problem $G|_e$

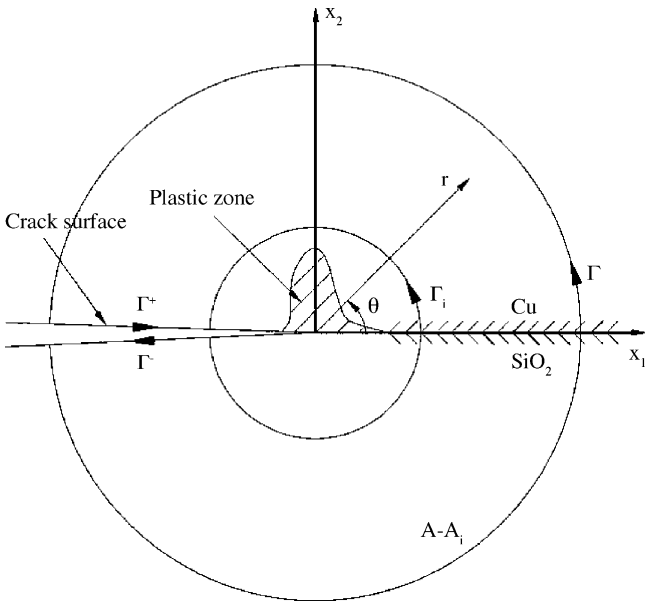


Fig. 4. The integral path and domain for the J -integral and the domain integral form of the J -integral.

$$G|_e = J = \frac{(c_1 + c_2)\mathbf{K}\bar{\mathbf{K}}}{16 \cos h^2 \epsilon \pi} \tag{5.a}$$

with

$$c_1 = \frac{\kappa_1 + 1}{\mu_1}, \quad c_2 = \frac{\kappa_2 + 1}{\mu_2} \tag{5.b}$$

The measure of the relative amount of the shear stress to the normal stress ahead of an interfacial crack tip along the interface, i.e., the phase angle is written, using the real part K_1 and the imaginary part K_2 of the complex interfacial stress intensity factor \mathbf{K} as:

$$\begin{aligned} \psi &= \tan^{-1} \left(\frac{\sigma_{12}}{\sigma_{22}} \right)_{r=\hat{r}} = \tan^{-1} \left(\frac{\text{Im}[\mathbf{K}\hat{r}^{i\epsilon}]}{\text{Re}[\mathbf{K}\hat{r}^{i\epsilon}]} \right) \\ &= \tan^{-1} \left(\frac{K_1 \cos \xi - K_2 \sin \xi}{K_1 \sin \xi + K_2 \cos \xi} \right) \end{aligned} \tag{6}$$

where $\xi = \epsilon \ln \hat{r}$, and \hat{r} is a reference length.

5. Elastic–plastic fracture analysis

When the plastic zone is developed near an interfacial crack tip, the stress and displacement fields in the elastic region outside the plastic zone include, not only the stress singularity $-1/2 + i\varepsilon$, but also the higher order singularities, such as, -1 , $-3/2 + i\varepsilon$, -2 , \dots [27–29], which are written as:

$$\begin{aligned} \sigma_{ij} = & \sum_{n=-\infty, \dots, -2}^{0, 2, \dots, \infty} \frac{r^{Re\delta_n}}{\sqrt{2\pi}} (Re[\mathbf{K}_n r^{i\varepsilon}] p_{ij}(\theta, Re\delta_n, \varepsilon) \\ & + Im[\mathbf{K}_n r^{i\varepsilon}] q_{ij}(\theta, Re\delta_n, \varepsilon)) \\ & + \sum_{n=-\infty, \dots, -1}^{1, \dots, \infty} \frac{r^{\delta_n}}{\sqrt{2\pi}} Re[\mathbf{K}_n] s_{ij}(\theta, \delta_n, \varepsilon) \end{aligned} \quad (7)$$

$$u_i = \frac{1}{2\mu} \left\{ \sum_{n=-\infty, \dots, -2}^{0, 2, \dots, \infty} \frac{r^{Re\delta_n+1}}{\sqrt{2\pi}} (Re[\mathbf{K}_n r^{i\varepsilon}] m_i(\theta, Re\delta_n, \varepsilon) + Im[\mathbf{K}_n r^{i\varepsilon}] n_i(\theta, Re\delta_n, \varepsilon)) + \sum_{n=-\infty, \dots, -1}^{1, \dots, \infty} \frac{r^{\delta_n+1}}{\sqrt{2\pi}} Re[\mathbf{K}_n] o_i(\theta, \delta_n, \varepsilon) \right\} \quad (8)$$

where $\mathbf{K}_n = K_{1n} + iK_{2n}$ are the complex interfacial stress intensities for each eigenvalue δ_n . The general solutions for p_{ij} , q_{ij} , s_{ij} , m_i , n_i and o_i are given by Jeon [28]. Note that eigenvalues δ_n are given as \dots , $\delta_{-2} = -3/2 + i\varepsilon$, $\delta_{-1} = -1$, $\delta_0 = -1/2 + i\varepsilon$, $\delta_1 = 0$, $\delta_2 = 1/2 + i\varepsilon$, \dots , and $Re\delta_n$ represent the real part of complex eigenvalues δ_n . For a crack problem, there should be complementary pairs of eigenvalues δ_n and δ_n^c in the J -integral sense [30] that satisfy the relation:

$$\delta_n + \delta_n^c = -1 \quad (9)$$

Therefore, for an arbitrary eigenvalue δ_n , the complementary eigenvalue $\delta_n^c = -1 - \delta_n$ has to be found in a crack problem.

From substituting the stress and displacement fields, including the higher order singularities in Eqs. (7) and (8) into the definition of the J -integral in Eq. (4) and some algebra considering the complementary relations for eigenvalues δ_n in Eq. (9) and the path independence characteristic of the J -integral, the energy-release rate for an elastic–plastic interfacial crack problem $G|_{ep}$ can be written as:

$$G|_{ep} = J = J_0 + \sum_{n=-1}^{\infty} J^{(\delta_n, \delta_n^c)} \quad (10)$$

where, $J^{(\delta_n, \delta_n^c)}$ is the two-state J -integral [31], that is, the mutual interaction integrals for arbitrary two elastic states of eigenvalues δ_n and δ_n^c . The term J_0 in Eq. (10) is the J -integral calculated with the eigenvalue $\delta_0 = -1/2 + i\varepsilon$, which has the same form as Eq. (5.a) [28]:

$$J_0 = \frac{1}{2} J^{(-1/2+i\varepsilon, -1/2-i\varepsilon)} = \frac{(c_1 + c_2)\mathbf{K}_0 \bar{\mathbf{K}}_0}{16 \cos h^2 \varepsilon \pi} \quad (11)$$

where \mathbf{K}_0 is the complex interfacial stress intensity factor for the eigenvalue $\delta_0 = -1/2 + i\varepsilon$.

6. Results and discussion

First of all, the determined dimensions and the reference geometric variables of the G_c -sensing element and the elastic behavior of the Cu thin film are used for calculating the reference energy-release rate G_0^e and phase angle Ψ_0 under the reference external loading $d_0 = 80 \mu\text{m}$. The perfect adhesion between the dissimilar materials is assumed and the residual stress of the Cu film is ignored because of its small magnitude compared with the stress distribution in the film driven by the external loading [16]. The finite element meshes, that consist of the isoparametric plane strain elements with eight nodes for the G_c -sensing element, as well as the indenter, are shown in Fig. 5a with boundary conditions. However, the small metal contact pad on the substrate is not included in the meshes for the simplicity of the computation. The pack-

age code ABAQUS is used for the convenience and the easy access to obtain the complex interfacial stress intensity factor \mathbf{K} and the energy-release rate $G|_e$ in Eq. (5.a). It provides the interaction integral method for obtaining those fracture parameters [32]. As a result of the numerical analysis, the deformed shape around the crack tip is presented in Fig. 5b. The zoomed shape around the crack tip shows the opened crack shape after the indentation process, which means the feasibility of the crack propagation between the Cu film and the SiO₂ layer.

The calculated energy-release rates and phase angles, non-dimensionalized by G_0^e and Ψ_0 , respectively, are presented in Fig. 6a along with the increase of the external loading d/d_0 . The phase angle ψ is calculated from Eq. (6) with the reference length $\hat{r} = 400 \text{ nm}$, selected the film thickness. The obtained energy-release rates $G|_e/G_0^e > 1$ with $G_0^e = 1.121 \text{ J/m}^2$ and the phase angle $\Psi_0 = -8.238^\circ$ insensitive to the increase of the external loading in Fig. 6a should be used for comparing with the measured interfacial toughness from the superlayer test, $0.7 \text{ J/m}^2 < G_c < 0.9 \text{ J/m}^2$ at the phase angle $\Psi \approx 0^\circ$ for the Cu film with a thickness of 450 nm [11]. From this comparison, it is confirmed that the G_c -sensing element can be utilized for measuring the interfacial toughness between the Cu film and the SiO₂ layer, using the microindenter. Fig. 6b shows the dependence of calculated energy-release rates and phase angles on the non-dimensionalized crack length, $2a/L_0$. The sudden decrease of the energy-release rate after the monotonic increase in Fig. 6b indicates the stability of the G_c -sensing element as a test specimen, because this behavior of the energy-release rate means the stationary crack after its propagation under the constant external loading. The reason for the sudden decrease of the energy-

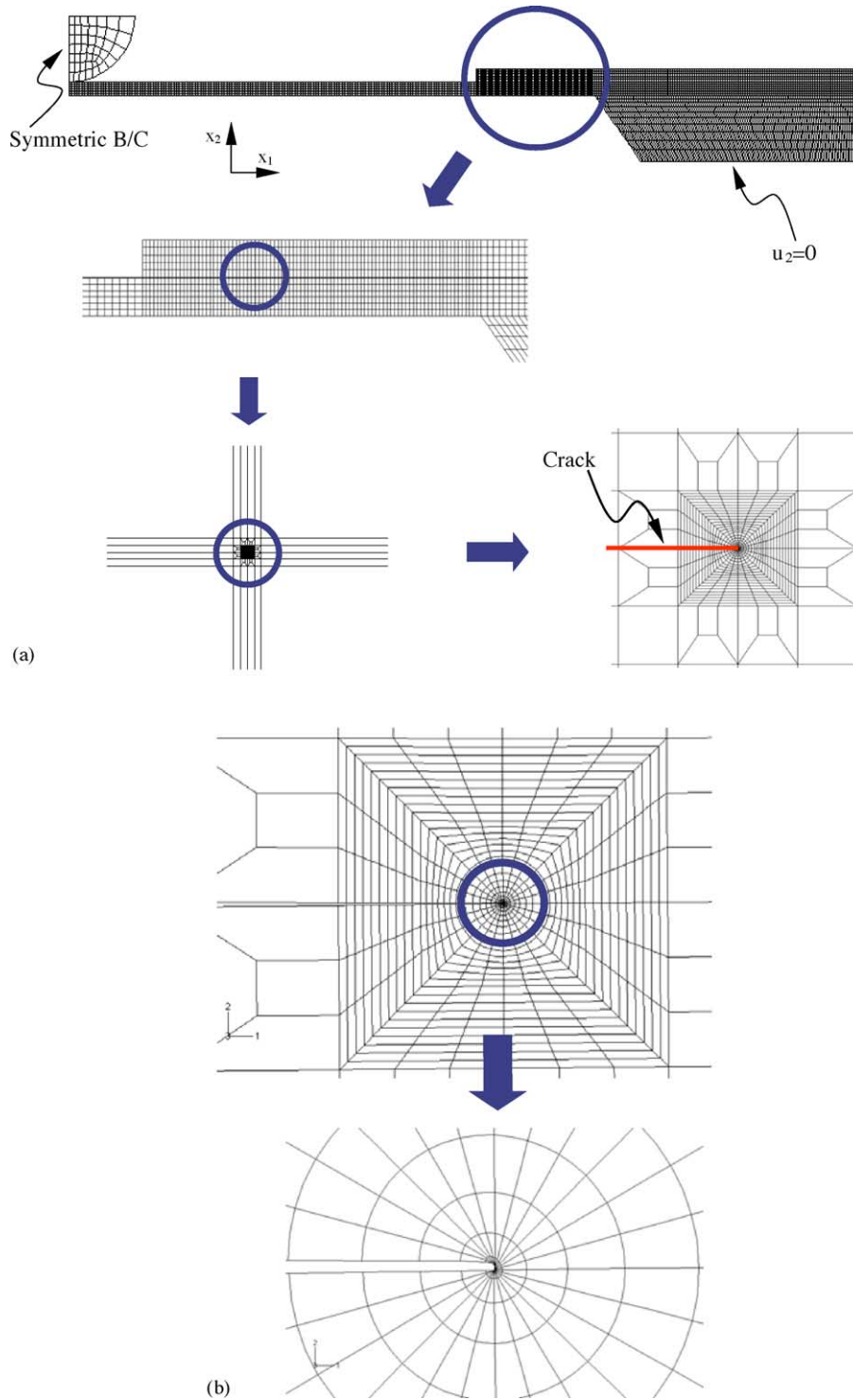


Fig. 5. (a) The mesh configuration and boundary condition for the G_c -sensing element, and (b) the deformed shape around the crack tip after the calculation.

release rate can be explained with the decrease of the phase angle along with the increase of the crack length in Fig. 6b, which means the decrease of the shear stress ahead of the crack tip that has the strong effect on the energy-release rate.

Fig. 7a and b shows the results of the parametric study using two selected variables, such as the thickness t^s and the

elastic modulus E^s of the SU8 layer. The values t^s and E^s can be determined by the fabrication process of the G_c -sensing element. For example, the viscosity of SU8 and the spinning velocity during the spin-coating process affect the thickness of the SU8 layer. Also, the time and temperature during the baking processes for SU8 affect the elastic modulus of the

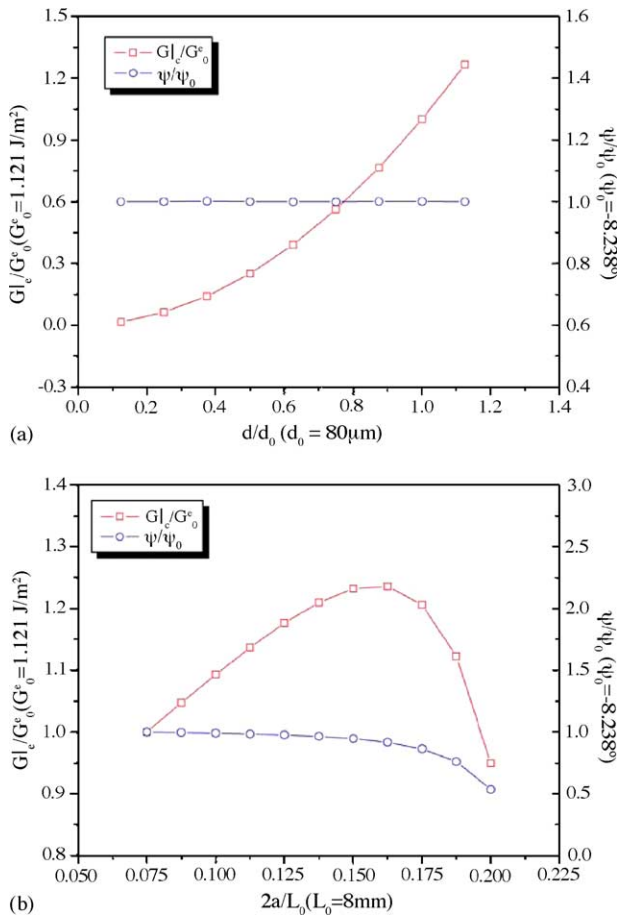


Fig. 6. Energy-release rates and phase angles, along with (a) the increase of the external loading, and (b) the crack length ($d_0 = 80\mu\text{m}$).

SU8 layer [22]. Fig. 7a shows the calculated energy-release rate range 0.3129–2.428 J/m² for the thickness range of the SU8 layer 50–150 μm under the external loading $d_0 = 80\mu\text{m}$. This result provides the possibility to obtain various practical energy-release rates for metal thin films through the G_c -sensing element with increasing the thickness of the SU8 layer. Particularly for SU8, over 300 μm thickness layer can be formed, using the spin-coating process. The increasing trend of the energy-release rate along with the increase of the SU8 layer thickness in Fig. 7a shows a good agreement with the results about the Cr layer thickness obtained from the superlayer test [11]. Fig. 7b shows the serious change of the phase angle, following the change of the elastic modulus of the material layered on the metal thin film. It means that the determination of the material type or property layered on the film for the G_c -sensing element gives the various values of the phase angle. Therefore, from these results, it is clarified that the G_c -sensing element can be an important implement to measure the interfacial toughness of various metal thin films on substrates.

For the verification of energy-release rates, calculated from the linear elastic fracture analysis, using the G_c -sensing element, the analysis considering the elastic–plastic behav-

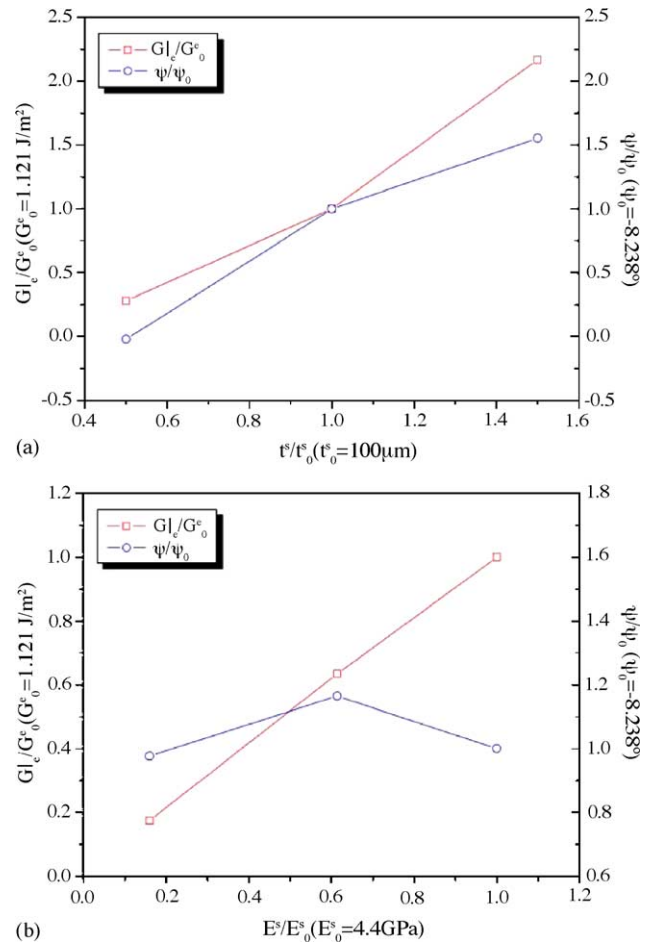


Fig. 7. Energy-release rates and phase angles, along with (a) the increase of the thickness, and (b) the elastic modulus of the SU8 layer ($d_0 = 80\mu\text{m}$).

ior of the Cu film is carried out. It is assumed that the Cu film follows the Prandtl–Reuss equations for the incremental plasticity theory of isotropic-hardening materials, and the calculation of the equations is processed with the plastic part of the Ramberg–Osgood model, using the power-law hardening exponent $n = 10$ [28,29]. Fig. 8 shows plastic zone shapes near the crack tip, non-dimensionalized by the film thickness $t = 400\text{nm}$ before the evolution to the fully plastic state, following the external loading d/d_0 .

The J -integral of the elastic–plastic crack problem in Eq. (10) is calculated as a domain integral form [28,29] using ABAQUS. The value J_0 in Eq. (10) is calculated from Eq. (11), with the obtained complex interfacial stress intensity factor K_0 from ABAQUS. Note that each calculation is carried out in the elastic region outside the plastic zone, i.e., $A - A_i$ region, shown in Fig. 4. The each term obtained in Eq. (10), along with the increase of the external loading d/d_0 , is arranged and compared with $G|_e$ in Table 2. The results in Table 2 show a good agreement between $G|_e$ and $G|_{ep}$, even though the large plastic zone is developed at $d/d_0 = 1.125$ near the crack tip (see Fig. 8). Certainly, this agreement stems from the geometric structure of the G_c -sensing element, because

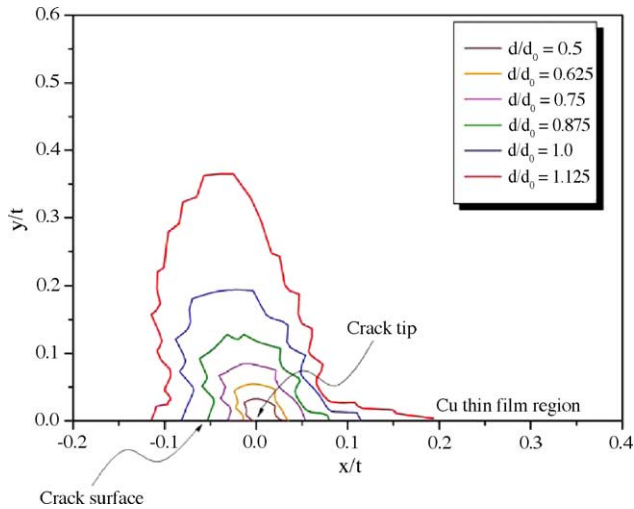


Fig. 8. Plastic zone shapes near the crack tip, non-dimensionalized by the film thickness $t = 400$ nm, before the evolution to fully plastic state.

Table 2

The energy-release rate $G|_e$ and each term in Eq. (10) along with the increase of the external loading d/d_0

d/d_0	$G _e$	J_0	$\sum_{n=-1}^{-\infty} J^{(\delta_n, \delta_n^c)}$	$G _{ep}$
0.125	0.01751	0.01753	-0.00001	0.01752
0.25	0.07005	0.07018	-0.0001	0.07008
0.375	0.1576	0.1581	-0.0004	0.1577
0.5	0.2802	0.2817	-0.0014	0.2803
0.625	0.4379	0.4413	-0.0034	0.4379
0.75	0.6305	0.6377	-0.0072	0.6305
0.875	0.8582	0.8725	-0.0141	0.8584
1	1.121	1.148	-0.026	1.122
1.125	1.419	1.47	-0.049	1.421

its deformation behavior during the indentation process is close to that of the middle tension (MT) specimen in which the small effect of $\sum_{n=-1}^{-\infty} J^{(\delta_n, \delta_n^c)}$ on the J -integral for the elastic–plastic crack problem exists, rather than that of the single-edge notched tension (SENT) specimen, in which the serious effect of $\sum_{n=-1}^{-\infty} J^{(\delta_n, \delta_n^c)}$ appears [29]. Therefore, this fact indicates that though the large-scale plastic zone is developed near the crack tip, the simple elastic analysis is sufficient to measure the interfacial toughness of metal thin films on substrates using the G_c -sensing element.

7. Conclusion and further study

The G_c -sensing element, that can be fabricated using the plain and general micro-fabrication process for measuring the interfacial toughness G_c of metal thin films on substrates, is proposed and modeled with the finite element method and the concepts of the linear elastic fracture mechanics.

From the comparison of calculated energy-release rates and phase angles with the measured ones of the superlayer test, and the obtained results from the parametric study with

the change of the thickness and elastic modulus of the SU8 layer, it is clarified that the G_c -sensing element is applicable for measuring the interfacial toughness of metal thin films on substrates. Furthermore, the simplicity for calculating the energy-release rate, using the G_c -sensing element, is confirmed from the verification with the elastic–plastic fracture analysis. Therefore, it is concluded that the G_c -sensing element provides a simple and convenient method for measuring the precise interfacial toughness of metal thin films on substrates.

For the further study, the fabrication of the G_c -sensing element with various metal thin films on the substrate and the measurement of the interfacial toughness using the G_c -sensing element are now in progress, and the results will be presented in the near future.

Acknowledgments

I. Jeon thanks Dr. Hyon-Jeong Lee for helpful and valuable discussions. This work was supported by the Post-Doctoral Fellowship Program of Korea Science & Engineering Foundation (KOSEF).

References

- [1] A.A. Griffith, The phenomena of rupture and flow in solids, *Phil. Trans. R. Soc. London A221* (1920) 163–198.
- [2] A.A. Volinsky, N.R. Moody, W.W. Gerberich, Interfacial toughness measurements for thin films on substrates, *Acta Mater.* 50 (2002) 441–466.
- [3] D.B. Marshall, A.G. Evans, Measurement of adherence of residually stressed thin films by indentation, *J. Appl. Phys.* 56 (1984) 2632–2638.
- [4] L.G. Rosenfeld, J.E. Ritter, T.J. Lardner, M.R. Lin, Use of the micro-indentation technique for determining interfacial fracture energy, *J. Appl. Phys.* 67 (1990) 3291–3296.
- [5] M.P. De Boer, W.W. Gerberich, Microedge indentation of the thin film fine line-I mechanics, *Acta Mater.* 44 (1996) 3169–3175.
- [6] J.J. Vlassak, M.D. Drory, W.D. Nix, A simple technique for measuring the adhesion of brittle films to ductile substrates with application to diamond-coated titanium, *J. Mater. Res.* 12 (1997) 1900–1910.
- [7] M.R. Begley, D.R. Mumm, A.G. Evans, J.W. Hutchinson, Analysis of a wedge impression test for measuring the interface toughness between films/coatings and ductile substrates, *Acta Mater.* 48 (2000) 3211–3220.
- [8] S. Venkataraman, D. Kohlstedt, W.W. Gerberich, Microscratch analysis of the work of adhesion for Pt thin films on NiO, *J. Mater. Res.* 7 (1992) 1126–1132.
- [9] N.R. Moody, R. Hwang, S. Venkataraman, J. Angelo, D. Norwood, W.W. Gerberich, Adhesion and fracture of tantalum nitride films, *Acta Mater.* 46 (1998) 585–597.
- [10] A. Bagchi, G. Lucas, Z. Suo, A.G. Evans, A new procedure for measuring the decohesion energy for thin ductile films on substrates, *J. Mater. Res.* 9 (1994) 1734–1742.
- [11] A. Bagchi, A.G. Evans, Measurement of the debond energy for thin metallization lines on dielectrics, *Thin Solid Films* 286 (1996) 203–212.
- [12] A. Kinbara, E. Kusano, T. Kamiya, I. Kondo, O. Takenaka, Evaluation of adhesion strength of Ti films on Si(110) by the internal stress method, *Thin Solid Films* 317 (1998) 165–168.

- [13] G. Xu, M.Y. He, D.R. Clarke, The effect of moisture on the fracture energy of TiN/SiO₂ interfaces in multi-layer thin films, *Acta Mater.* 47 (1999) 4131–4141.
- [14] S. Johansson, J. Shuweiz, L. Tenerz, J. Tiren, Fracture testing of silicon microelements in situ in a scanning electron microscope, *J. Appl. Phys.* 63 (1988) 4799–4803.
- [15] Y.R. Kang, S.C. Kang, K. Paek, Y.K. Kim, S.W. Kim, B.K. Ju, Air-gap type film bulk acoustic resonator using flexible thin substrate, *Sens. Actuators A* 117 (2005) 62–70.
- [16] T. Kitamura, H. Hirakata, T. Itsuji, Effect of residual stress on delamination from interface edge between nano-films, *Eng. Fract. Mech.* 70 (2003) 2089–2101.
- [17] A.V. Zhuk, A.G. Evans, J.W. Hutchinson, The adhesion energy between polymer thin films and self-assembled monolayers, *J. Mater. Res.* 13 (1998) 3555–3564.
- [18] B.J. Kim, M. Liebau, J. Huskens, D.N. Reinhoudt, J. Brugger, A self-assembled monolayer-assisted surface microfabrication and release technique, *Microelectron. Eng.* 57–58 (2001) 755–760.
- [19] J.M. Ambrico, M.R. Begley, The role of flaw geometry in thin film delamination from two-dimensional interface flaws along free edges, *Eng. Fract. Mech.* 70 (2003) 1721–1736.
- [20] T. Yi, C.J. Kim, Measurement of mechanical properties for MEMS materials, *Meas. Sci. Technol.* 10 (1999) 706–716.
- [21] Y.B. Park, I. Jeon, Mechanical stress evolution in metal interconnects for various line aspect ratios and passivation dielectrics, *Microelectron. Eng.* 69 (2003) 26–36.
- [22] R. Feng, R.J. Farris, Influence of processing conditions on the thermal and mechanical properties of SU8 negative photoresist coatings, *J. Micromech. Microeng.* 13 (2003) 80–88.
- [23] J.R. Rice, Elastic fracture mechanics concepts for interfacial cracks, *ASME J. Appl. Mech.* 55 (1988) 98–103.
- [24] J.W. Hutchinson, Z. Suo, Mixed mode cracking in layered materials, *Adv. Appl. Mech.* 29 (1992) 63–191.
- [25] J.R. Rice, Z. Suo, J.S. Wang, Metal–ceramic interfaces, in: *Mechanics and Thermodynamics of Brittle Interfacial Failure in Bimaterial Systems*, Pergamon Press, New York, 1990, pp. 269–294.
- [26] J.R. Rice, A path-independent integral and the approximate analysis of strain concentration by notches and cracks, *ASME J. Appl. Mech.* 35 (1968) 379–386.
- [27] C.Y. Hui, A. Ruina, Why K? High order singularities and small-scale yielding, *Int. J. Fract.* 72 (1995) 97–120.
- [28] I. Jeon, The higher order singularities and their energetics in elastic–plastic crack tips, Ph.D. Dissertation, Korea Advanced Institute of Science and Technology (KAIST), 2000.
- [29] I. Jeon, S. Im, The role of higher order eigenfields in elastic–plastic cracks, *J. Mech. Phys. Solids* 49 (2001) 2789–2818.
- [30] S. Im, K.S. Kim, An application of two-state *M*-integral for computing the intensity of the singular near-tip field for a generic wedge, *J. Mech. Phys. Solids* 48 (2000) 129–151.
- [31] F.H.K. Chen, R.T. Shield, Conservation laws in elasticity of the *J*-integral type, *Z. Angw. Math. Phys.* 28 (1977) 1–22.
- [32] ABAQUS Standard User’s Manual 6.2.